This is the accepted manuscript of

VUV Photoionization Measurements and Electronic Structure Calculations of the Ionization Energies of Gas-Phase Tantalum Oxides TaO_x (x=3-6)

Manori Perera, Kevin M. Roenitz, Ricardo B. Metz, Oleg Kostko and Musahid Ahmed*

It is provided for the convenience of those who do not have access to the journal.

Please cite it as

Journal of Spectroscopy and Dynamics volume 4, article number 21 (10 pages) (2014).

VUV Photoionization Measurements and Electronic Structure Calculations of the Ionization Energies of Gas-Phase Tantalum Oxides TaO_x (x=3-6)

Manori Perera,[a] Kevin M. Roenitz,[a] Ricardo B. Metz,[b] Oleg Kostko[c] and Musahid Ahmed[c]*

a) Dept. of Chemistry, Illinois Wesleyan University, Bloomington, IL 61702 USA

b) Dept. of Chemistry, University of Massachusetts Amherst, Amherst, MA 01003 USA

e-mail: rbmetz@chem.umass.edu

c) Chemical Sciences Division, Lawrence Berkeley National Laboratory, Berkeley, CA 94720 USA

Abstract

Photoionization efficiencies (PIE) were measured for TaO_x (x=3-6) via single-photon ionization using tunable VUV from a synchrotron. The PIEs were compared to simulations based on candidate structures for neutrals and cations calculated at the B3LYP/aug-cc-pVTZ level to assign ground state structures for the neutrals and determine ionization energies. TaO_3 shows a sharp photoionization onset, which a harmonic normal mode analysis fails to reproduce. Calculations predict that TaO_3 and TaO_3^+ have pseudo-C_{3v} symmetry, with distortions along two degenerate antisymmetric Ta-O stretches. Modeling this distortion using calculated coupled anharmonic 2D potentials leads to a much sharper predicted PIE onset, in excellent accord with the experiment, with IE(TaO_3)=10.65±0.05 eV. The PIE of TaO_4 shows a more gradual onset, and is due to ionization of the ground, superoxide structure to a similar superoxide form of TaO_4^+, with an ionization energy of 10.53±0.05 eV. This is calculated to lie 0.17 eV above the ground state of TaO_4^+, in which O_2 is electrostatically bound to TaO_2^+. The adiabatic IE(TaO_4) is thus 10.36±0.1 eV. TaO_5 and TaO_6 show gentle onsets and slightly lower ionization energies. The calculations predict a (η^2-O_2) TaO_3 superoxide structure for TaO_5. However, this is not consistent with the measured PIE, which supports a (η^1-O_2) TaO_3 dioxygen structure, with IE(TaO_5)=10.0±0.2 eV. A similar situation occurs for TaO_6. Although our calculations predict a bis(η^2-O_2) TaO_2 structure, the relatively sharp observed PIE clearly favors a (η^2-O_2)(η^1-O_2) TaO_2 structure, with an ionization energy of 10.10±0.05 eV.

Keywords: photoionization, tantalum oxides, superoxide

I. Introduction

Oxides of the group V metals, vanadium, niobium and tantalum, are widely used, flexible catalysts due to the ability of the metals to adopt a range of oxidation states and a variety of oxygen binding motifs (single and multiple metal-oxo, superoxide, peroxy). Although they have been less extensively investigated than oxides of the other group V metals, tantalum oxides, especially when supported on other metal oxides[1, 2] or doped into zeolites[3, 4], have shown promising catalytic activity and selectivity, particularly for oxidations.

The catalytic utility of tantalum oxides has led to several gas-phase studies of their structure and reactivity. Bernstein and coworkers characterized the Ta_nO_x neutrals produced by laser ablation of Ta foil in an expansion of 5% O_2 in He by detecting ions formed by ionization at three photon energies. At 6.4 eV, they observe Ta^+, TaO^+ and TaO_2^+, all formed by multiphoton ionization. At 10.5 eV, TaO^+ dominates, while at 26.5 eV TaO_2^+ is the most intense mono-tantalum ion, but substantial amounts of TaO_3^+ are also observed, along with small amounts of TaO^+, TaO_4^+ and TaO_5^+.[5] They subsequently studied reactions of these neutral clusters, observing that oxygen-rich clusters, especially TaO_3, efficiently oxidize NO, forming complexes such as $TaO_2(NO_2)$.[6] In addition, Zhou and coworkers find that TaO_4 activates H_2, even at cryogenic temperatures. They propose TaO_4 as a model catalyst for hydrogenation of formaldehyde to methanol.[7] Duncan and coworkers found that ablation of Ta in an expansion in 1-5% O_2 produces TaO_2^+, along with smaller amounts of TaO_x^+ (x=3-7) and many larger multi-metal clusters $Ta_nO_x^+$ (n=2-9; x=5-22). The multi-metal clusters photodissociate by loss of O or O_2.[8] Castleman and coworkers studied the reactions of TaO_x^+ (and larger clusters) with hydrocarbons, observing C-C bond cleavage as a major channel, which, for the very oxygen-rich clusters (x=4, 5) is accompanied by O_2 loss.[9]

The electronic spectrum of gas-phase TaO has been measured[10, 11] and there have been several matrix isolation studies of the electronic [12] and vibrational [13-16] spectroscopy of neutral and cationic tantalum oxides. Dyke and coworkers measured the ionization energy of TaO using high-temperature photoelectron spectroscopy[17] and Bowen and coworkers measured the photoelectron spectra of the TaO^-, TaO_2^- and TaO_3^- anions.[18]

The interesting reactivity, potential variety of oxygen binding motifs and limited electronic structure information available for the higher oxides prompted the present study of the photoionization of tantalum oxides TaO_x (x=3-6). Single-photon ionization of the higher oxides

requires tunable vacuum ultraviolet (VUV) light at 10-11 eV. However, these refractory molecules can only be produced in low concentrations in the gas phase, tunable laboratory VUV sources are typically not sufficiently intense to produce useful ion signals, while resonant two-color, two-photon ionization is a challenge due to the uncharacterized electronic spectroscopy, high ionization energies and low dissociation energies of the higher oxides. Thus, the experiments were carried out using a synchrotron where intense, tunable VUV is readily available.

II. Experimental

The photoionization experiments were performed at the Chemical Dynamics Beamline at the Advanced Light Source (ALS) at Lawrence Berkeley National Laboratory.[19-22] As in our previous studies of transition metal oxides FeO, CuO,[23] PtO and PtO_2,[24] the molecules of interest are produced using a pulsed laser ablation source and ionized using VUV light. The resulting ions are extracted into a reflectron time-of-flight mass spectrometer and tallied with a fast counter. Photoionization efficiency curves (PIE) are measured by integrating the area under the photo-ion of interest and normalizing to ALS current and VUV flux.

Laser ablation (Nd:YAG laser at 532 nm; 50 Hz repetition rate) of a tantalum rod produces tantalum atoms that then react with oxygen gas from a pulsed piezoelectric valve. The molecules cool in the supersonic expansion. The molecular beam is skimmed and the neutral molecules are irradiated by VUV light. The beamline provides vacuum ultraviolet (VUV) light with photon energies of 8-16 eV at a repetition rate of 500 MHz. The spectral line width is determined by the slit width on a 3 meter monochrometer. A pulsed voltage extracts neutrals that are ionized by the VUV light into a time-of-flight reflectron mass spectrometer. Masses of photo-ions are determined by their flight times to a dual micro channel plate detector.

Mass spectra are obtained as a function of VUV photon energy, typically summing signal over 8000 laser shots at each energy. Photoionization efficiency curves (PIE) are measured by integrating the area under the photo-ion of interest and normalizing to ALS current and VUV flux as measured by a Si photodiode. Survey scans (not shown) with 1500 μm slit width are used to identify the products and estimate the onset region for each. Finer scans, with 1000 μm slits (~45 meV at 10.5 eV), near each onset are used to determine ionization energies. Although two charged plates deflect ions produced in the laser ablation source so that they do not pass

through the skimmer, a small number of ions does leak into the VUV interaction region, producing background counts. This background is removed from the PIE spectrum by subtracting off the background counts just before and just after the ion of interest in the mass spectrum. Error bars in the PIE are based on counting statistics.

Electronic structure calculations were carried out with the *Gaussian09* electronic structure package[25] using hybrid density functional theory with the B3LYP functional. The aug-cc-pVTZ-PP relativistic effective core potential and basis set[26] was used for tantalum; the aug-cc-pVTZ basis set was used for oxygen. Harmonic frequencies were calculated at each stationary point to ensure that it is a minimum. The resulting frequencies were not scaled. All reported energies include the zero-point contribution.

III. Results

Figure 1 shows survey photoionization efficiency (PIE) spectra of TaO_3, TaO_4, TaO_5 and TaO_6. Very little TaO^+ or TaO_2^+ signal was observed, so useful PIEs could not be obtained. TaO_3 and TaO_4 have the highest, and sharpest, onsets. However, all four observed onsets are fairly similar, and are well above the ionization energies of TaO (8.61 eV)[17] and TaO_2 (8.5±0.5 eV;[27] 9.0±0.5 eV).[28] The PIEs of the tantalum oxides will be analyzed and results of calculations of the structures and vibrations of the neutrals and cations will be discussed in turn.

IV. Analysis and Discussion

A. TaO

Very little TaO^+ was observed, even well above IE(TaO)=8.61 eV.[17] For TaO, our calculations predict a $^2\Delta$ ground state with r_e=1.680 Å, ω_e=1049 cm^{-1} and D_0=8.12 eV (structure **1**, Fig. 2) in good accord with the experimental values: r_e=1.687 Å, ω_e=1030 cm^{-1} [10, 11] and D_0=8.30±0.13 eV;[27] 8.19 eV.[29] The calculated dissociation and ionization energies have not been corrected for spin-orbit effects. The spin-orbit splittings are similar for Ta, Ta^+ and TaO and have not been measured for TaO^+, so this correction would only have a small effect on the calculated values. For TaO^+, our calculations predict a $^3\Delta$ ground state with r_e=1.658 Å and ω_e=1086 cm^{-1}, again in good accord with values measured by Cheetham and Barrow[10] and tentatively attributed to TaO^+: r_e=1.667 Å and ν_0=1051 cm^{-1}. The calculated ionization energy of TaO is 7.93 eV (Table 1), which is somewhat below IE(TaO)=8.61±0.02 eV measured via high-

temperature photoelectron spectroscopy.[17] Our calculated value agrees with previous B3LYP results obtained with smaller basis sets.[30] A similar discrepancy is also present in $D_0(Ta^+\text{-}O)$, with the calculated value (7.66 eV; Table 2) somewhat higher than the value measured via guided ion beam mass spectrometry: 7.01±0.12 eV.[31, 32] The dissociation and ionization energies are linked via a thermodynamic cycle:

$$D_0(TaO)=D_0(Ta^+\text{-}O) + IE(TaO) - IE(Ta) \quad (1)$$

with IE(Ta)=7.54957 eV.[33] The independent experimental measurements are consistent with this cycle, so the discrepancy between the experimental and calculated values is due to inadequacies in the B3LYP functional. Hinton et al.[32] provide a critical examination of the experimental and computational work on this system.

B. TaO_2

Little TaO_2^+ is observed, and a clear onset could not be determined. Our calculations predict that neutral TaO_2 has a $^2A_1$ ground state with r_{TaO}=1.719 Å and ∠O-Ta-O=105.9° (structure **2**, Fig. 2). The bond angle agrees with the value of 106±5° obtained via isotopic substitution in the matrix isolation study of Zhou and Andrews.[13] The calculated vibrational frequencies are about 4% higher than the observed matrix values (ν_1=965.3 cm^{-1} and ν_3=906.9 and 912.2 cm^{-1}).[13, 14] The TaO_2 ν_1 vibration is also observed at 0.12 eV (~968 cm^{-1}) in the photoelectron spectrum of TaO_2^-.[18] The geometry is similar to that calculated by Zhou and Andrews[13] using the BP86 functional and by Chen et al.,[14] using the B3LYP functional each with the D95* basis on O and LANL2DZ basis on Ta, although our calculated frequencies are slightly higher. TaO_2^+ has a $^1A_1$ ground state with r_{TaO}=1.688 Å and ∠O-Ta-O=103.9° (structure **2c**). Again, the bond angle agrees with the value of 105±5° obtained by Zhou and Andrews.[13] The calculated vibrational frequencies are 6% higher than the matrix values (ν_1=993.1 cm^{-1} and ν_3=937.4 and 938.8 cm^{-1}).[13, 14]. The lowest triplet state ($^3B_2$) is calculated to lie 149 kJ/mol above the $^1A_1$. The ionization energy is calculated to be 8.80 eV. The calculations predict that the OTa-O bond is extremely strong, D_0=7.04 eV, in good agreement with high temperature equilibrium measurements (Table 1).[27, 29] The OTa^+-O bond is somewhat weaker, but still exceeds the 5.45 eV OC-O bond strength, in accord with observed[34] oxygen abstraction from

CO_2 by TaO^+. The calculated value (D_0=6.18 eV) is in excellent agreement with the results of guided ion beam measurements (6.08±0.12 eV).[32]

C. TaO_3

The photoionization efficiency spectrum of TaO_3 shows a sharp onset at 10.65-10.7 eV (Fig. 3). This continues the trend of increasing ionization energies with additional bonds to oxygen observed in going from Ta (7.55 eV)[33] to TaO (8.61 eV)[17] to TaO_2 (8.5±0.5 eV;[27] 9.0±0.5 eV).[28] Our calculations predict that TaO_3 has a doublet ground state with a distorted trigonal pyramidal structure, with two Ta=O double bonds (1.747 Å) and one Ta-O single bond (1.884 Å), resulting in C_s symmetry (structure **3**, Fig. 2). The TaO_3^+ cation is predicted to have a triplet ground state, also with a distorted pyramidal structure, but with one Ta=O double bond (1.712 Å) and two Ta-O single bonds (1.846 Å) (**3c**, Fig. 2). The geometries of TaO_3 and TaO_3^+ are similar to those calculated for isoelectronic HfO_3^- and HfO_3 by Zhai et al.,[35] with five net metal-oxygen bonds in TaO_3/HfO_3^- and four in TaO_3^+/HfO_3.

Figure 3 shows the PIE of TaO_3 along with two simulated PIE spectra. They are calculated by computing the geometries and vibrations of the neutral and cation, and calculating Franck-Condon factors (FCFs) for each vibration. The products of the Franck-Condon factors are then integrated and convolved with the 45 meV VUV Gaussian linewidth to generate the PIE spectrum.[22, 36] The ionization energy is determined by shifting the energy origin of the simulation until it provides the best match to the measured PIE spectrum. The simulation shown with a dotted line is obtained by calculating FCFs assuming all vibrations are separable and harmonic. This simulation clearly predicts a more gentle onset than is observed experimentally.

The simple harmonic calculation neglects to consider that there are three equivalent C_s structures for each species, and that they can interconvert. These structures are most readily analyzed as arising from a C_{3v} trigonal pyramidal structure which has distorted by displacement along one of the two degenerate antisymmetric Ta-O stretch vibrations, Q_{3a} and Q_{3b}. These two vibrations are coupled and anharmonic, and they replace the O-Ta-O antisymmetric stretch and Ta-O stretch vibrations in the harmonic C_s calculation. The reference C_{3v} geometry and the displacements corresponding to each vibration are in Table 3. Figure 4 shows the potential along Q_{3a} and Q_{3b} for TaO_3 and TaO_3^+. For the neutral, the three equivalent minima are at (Q_{3a}, Q_{3b}) = (-0.1, 0.0), (0.05, $0.1\sqrt{3}$) and (0.05, $-0.1\sqrt{3}$). The minimum energy pathway between the minima

is via an asymmetrical C_1 structure with 100 cm^{-1} barrier. The symmetrical C_{3v} geometry (Q_{3a}, Q_{3b})=(0, 0), is 350 cm^{-1} above the minima. For the cation, the minima are at (0.1, 0.0), (-0.05, $0.1\sqrt{3}$) and (-0.05, $-0.1\sqrt{3}$). They can interconvert via an asymmetrical C_1 structure with 270 cm^{-1} barrier. The C_{3v} structure lies 870 cm^{-1} above the minima. In order to calculate the eigenvalues and wavefunctions for the two-dimensional potentials we calculate $V(Q_{3a}, Q_{3b})$ over a grid of points and fit a flexible functional form to the potential. This is simplest in polar coordinates. Let $r = \sqrt{Q_{3a}^2 + Q_{3b}^2}$ and $\theta = tan^{-1}\left(\frac{Q_{3a}}{Q_{3b}}\right)$. Then

$$V(r,\theta) = q\,r^3 + \frac{1}{2}k\,r^2 - a\,r - (b\,r^2 + c\,r + d)\,r^2\,cos(3\theta) \qquad (2)$$

This is an extension of the functional form used to fit the triple-minimum potential in NO_3.[37] As in the case of NO_3, the multi-minimum potential is likely due to Jahn-Teller and pseudo Jahn-Teller interactions between the ground and excited state(s).[38] The parameters q, k and a are determined by fitting calculated density functional energies E(r, θ=0)+E(r, θ=π), while b, c and d are obtained by fitting E(r, θ=0)-E(r, θ=π), from r=0 to 0.2 Å. The resulting parameters are shown in Table 4.

The Schrödinger equation for the two-dimensional potentials for the neutral and cation is solved variationally in the Q_{3a}, Q_{3b} coordinate system, using a particle-in-a-box basis set. Calculations are carried out in *Mathematica*. The ground state wavefunctions for TaO_3 and TaO_3^+ are shown in figure 4. For the neutral, the most probable antisymmetric stretch coordinate is (Q_{3a}, Q_{3b})= (0,0), which corresponds to the pyramidal C_{3v} geometry. For the cation, which has slightly deeper C_s minima, the most probable coordinate is slightly distorted C_s, but there is substantial amplitude at the C_{3v} geometry. As a result, the two-dimensional analysis predicts that photoionization of TaO_3 primarily produces TaO_3^+ in its antisymmetric stretch ground state (89%). Photoionization leads to a modest progression in the umbrella bend. The resulting simulated PIE, including the 45 meV VUV linewidth, is shown in Figure 3 (solid line). The simulation now does an excellent job of reproducing the observed, fairly sharp, onset, confirming that TaO_3 and TaO_3^+ effectively have trigonal pyramidal C_{3v} structures. Matching the onsets of the measured and simulated PIE spectra gives IE(TaO_3)=10.65±0.05 eV.

The two-dimensional calculations predict that the antisymmetric stretch fundamentals for TaO_3 are 239 cm^{-1} (ν_{3b}) and 240 cm^{-1} (ν_{3a}), while those for TaO_3^+ are 205 cm^{-1} (ν_{3b}) and 212 cm^{-1} (ν_{3a}). Overall, our computational results for TaO_3 are similar to those of Zhou and

Andrews, who predict a nearly trigonal structure with r_{Ta-O}=1.793 Å using the BP86 functional and a smaller basis set (D95* on O and LANL2DZ on Ta).[13] Wu et al. obtain a nearly identical geometry to ours for TaO_3, but predict that TaO_3^+ has C_{3v} symmetry, with r_{Ta-O}=1.796 Å.[30] Their calculation used the B3LYP functional, with a basis set similar to that of Zhou and Andrews (6-311+G(3df) on O and LANL2DZ on Ta). Although our calculations use the same B3LYP functional, they employ a larger, more flexible basis set. This has only a small effect on the geometries, and has little effect on the bond strengths for the smaller clusters. However, the larger basis set calculations predict somewhat stronger bonds for TaO_3 and, especially, TaO_3^+. As a result, our calculations predict IE(TaO_3)=10.50 eV, in better agreement with experiment than the 11.16 eV value calculated by Wu et al.

D. TaO_4

The photoionization efficiency spectrum of TaO_4 shows an onset at ~10.6 eV (Fig. 5). The onset is clearly more gentle than is observed for TaO_3, suggesting that photoionization leads to a modest structural change. Our calculations predict that TaO_4 is strongly bound, with a TaO_2-O_2 bond strength of 2.46 eV. The covalent nature is reflected in the structure as well (**4**, in Figure 6). The O-O bond length is 1.333 Å, which is substantially longer than in free O_2 (1.206 Å, at this level of theory), and is nearly identical to the value in the superoxide (O_2^- : 1.343 Å). Similarly, the O-O stretching frequency in TaO_4 is calculated to be 1168 cm^{-1}, compared to 1626 cm^{-1} in O_2 and 1164 cm^{-1} in O_2^-. Binding to the O_2 also affects the structure of the TaO_2 moiety, increasing r_{TaO} by 0.016 Å and ∠O-Ta-O by 5.2°. TaO_4 is thus formally a d^0 (η^2-O_2) Ta^VO_2 superoxide complex.[7] This species shows very promising reactivity. Zhou et al. observe that TaO_4 spontaneously activates H_2 at 25K in an argon matrix, forming H-TaO(OH) (η^2-O_2). They propose TaO_4 as a model catalyst for hydrogenation of formaldehyde to methanol.[7] In addition, tantalum doped onto a mesoporous SBA15 silica support is an effective catalyst for conversion of alkenes to epoxides using H_2O_2 as the oxidant. The active site is Ta(V) oxide centers, and a Ta(V) (η^2-O_2) intermediate has been observed by UV absorption.[3, 4]

Our calculations on TaO_4 give very similar results to those of Zhou and Andrews[13] and Zhao et al.[15] which also predict a superoxide structure. The argon matrix isolation IR spectra[13, 15] confirm the presence of two sets of symmetrical oxygens, with the O-O stretch observed at 1095.7 cm^{-1}, consistent with a superoxide. The calculations are also consistent with

the remaining vibrations observed: 946.3/950.5 cm^{-1} (O-Ta-O symmetric stretch, with two absorptions due to different matrix sites), 889.4/894.5 cm^{-1} (O-Ta-O antisymmetric stretch) and 524.2 cm^{-1} (Ta-(O_2) stretch). Similar frequencies were also observed by Chen et al.[14] In light of their later matrix isolation study which revealed further coordination of TaO_4 to Xe and O_2, Zhao et al. suggest that the complexes observed in an argon matrix are best regarded as TaO_4(Ar).[15]

Our calculations predict that the ground state of TaO_4^+ is $^3A''$ and corresponds to an electrostatic (η^1-O_2) TaO_2^+ complex (structure **4c_A**, Fig. 6). Binding to O_2 has little effect on the TaO_2^+ geometry, changing r_{TaO} by <0.01 Å and ∠O-Ta-O by only 0.3°. Similarly, binding to TaO_2^+ has little effect on the oxygen geometry, with a 0.001 Å change in bond length and a calculated 35 cm^{-1} reduction in its vibrational frequency. The TaO_2^+-O_2 bond strength is calculated to be 0.96 eV, consistent with an electrostatic complex. The calculated ionization energy of TaO_4 is 10.31 eV. However, the geometries of TaO_4 and the $^3A''$ state of TaO_4^+ are so different that simulations predict that the PIE should have an onset about four times as broad as is observed, and that the midpoint of the onset lies 1.5 eV above the adiabatic IE. Singlet and quintet states of TaO_4^+ are calculated to lie 1.3 and 2.0 eV above the $^3A''$ state, respectively, so they should not contribute to the spectrum below ~11.6 eV. Additional calculations reveal a $^3A'$ state of TaO_4^+ which lies 0.17 eV above the $^3A''$ state and has a superoxide structure similar to that of neutral TaO_4. This distorts slightly from C_s symmetry to give a ^3A structure in which the covalent Ta-O bond lengths differ by 0.15 Å, as shown in Fig. 6, structure **4c_B**. The antisymmetric O-Ta-O stretch potential is very flat, with the symmetrical, C_s configuration only ~80 cm^{-1} above the minimum, so this state will be referred to as the $^3A'$ state. The PIE for ionization of TaO_4 to the $^3A'$ state of TaO_4^+ was calculated, solving the Schrödinger equation numerically for the antisymmetric O-Ta-O stretch, and assuming the remaining vibrations are harmonic. This leads to the simulation shown in Fig. 5, which reproduces the shape of the experimental PIE. The best match between experiment and simulation corresponds to an adiabatic energy of 10.53±0.05 eV for ionization of TaO_4 to the $^3A'$ state of TaO_4^+. Since the $^3A'$ state lies 0.17 eV above the ground state, this corresponds to an adiabatic IE(TaO_4)=10.36±0.1 eV, where the larger error bars reflect the uncertainty in the calculated $^3A''$ - $^3A'$ splitting.

E. TaO_5

The PIE spectrum of TaO_5 shows a very gradual onset, indicating a large geometry change upon ionization (Fig. 7). A linear fit to the PIE near the onset (solid black line) gives an upper bound to the ionization energy of 10.17 eV. The calculations predict that neutral TaO_5 is a ^4A (η^2-O_2) TaO_3 superoxide complex (**5_A** in Fig. 8) with a geometry analogous to that of TaO_4. The calculations also predict a low-lying doublet state of TaO_5 at 0.04 eV. Its geometry is very similar to that of the ^4A ground state. In addition, η^1-O_2 dioxygen structures were explored. The lowest energy (η^1-O_2) TaO_3 state is a ^4A state (**5_B** in Fig. 8). It is calculated to lie 0.30 eV above the superoxide (**5_A**). Doublet (η^1-O_2) TaO_3 is calculated to lie 0.03 eV above quartet (η^1-O_2) TaO_3. The ground state of the TaO_5^+ cation is calculated to be a $^5A''$ (η^1-O_2) TaO_3^+ electrostatic complex (**5c** in Fig. 8). The lowest triplet state of TaO_5^+ is calculated to be 0.45 eV above the quintet. In addition, the calculations predict that superoxide structures of TaO_5^+ lie well above the ground state and thus should not contribute to the PIE below 11 eV.

The calculations predict a superoxide structure (**5_A**) for the neutral and a dioxygen structure (**5c**) for the cation. However, simulations of the PIE using these structures and harmonic vibrations predict an onset that is about twice as broad as is observed, due to extended vibrational progressions in the Ta-OO bend and stretch, and in the O-O stretch. In contrast, simulations, (dotted trace in Fig. 7) from the dioxygen structure of the neutral (**5_B**) reproduce the observed PIE spectrum. This is surprising, as the B3LYP calculations predict that the dioxygen structure of TaO_5 lies 0.30 eV above the superoxide. So, the relative energies of these two isomers of TaO_5 were calculated at the CCSD(T) level, using the aug-cc-pVTZ basis set, at the B3LYP geometry. These higher-level calculations give essentially the same result: the dioxygen structure is less stable by 0.29 eV. The simulated PIE of the dioxygen structure of TaO_5 gives an ionization energy of 9.8 eV. This likely represents a lower limit, as the simulated PIE has a slightly gentler onset than experiment, and the simulation predicts that the PIE doesn't noticeably increase until well above the adiabatic IE. Combining this lower limit with the upper limit of 10.17 eV from the linear fit near the onset (solid black line in Fig. 7) gives IE(TaO_5)=10.0±0.2 eV.

F. TaO_6

The photoionization efficiency spectrum of TaO_6 is shown in the lower trace of figure 7. The onset is narrower than for TaO_5, but is somewhat more gentle than is observed for TaO_4, again suggesting that photoionization leads to a modest change in geometry. A linear fit to the PIE near the onset (solid line) gives an upper limit of IE(TaO_6)=10.16 eV. Recent calculations by Zhao et al.,[15] using the B3LYP functional with the 6-311+G(3df) basis on O and SDD on Ta predict a TaO_6 structure with η^1-O_2 bound to TaO_4, resulting in a (η^2-O_2)(η^1-O_2) TaO_2 structure. Our calculations, using a larger basis set, predict a bis (η^2-O_2) TaO_2 ground state (**6_A** in Fig. 9), with the (η^2-O_2)(η^1-O_2) TaO_2 structure only 0.16 eV higher in energy (**6_B** in Fig. 9).

As with TaO_4^+ and TaO_5^+, the calculations predict that the ground state of TaO_6^+ is formed by taking the neutral and oxidizing one superoxide ligand to dioxygen. This results in a (η^2-O_2)(η^1-O_2) TaO_2^+ structure (**6c**). The ground state is predicted to be a quintet, although the triplet state is calculated to lie only 0.02 eV higher in energy. Di-superoxide structures analogous to that of the neutral were investigated, but are found to relax to the (η^2-O_2)(η^1-O_2) TaO_2^+ geometry.

The simulated PIE of the bis (η^2-O_2) TaO_2 ground state (**6_A**) of TaO_6 is about twice as broad as is observed. As with TaO_5, this is due to the large displacement along the Ta-O-O bend and O-O stretch in converting an η^2 superoxide to η^1 dioxygen. Although triplet TaO_6^+ is nearly degenerate with the quintet state, its geometry differs slightly more from that of the neutral, hence the simulated PIE to the triplet state is even broader. In contrast, simulations of the PIE from the (η^2-O_2)(η^1-O_2) TaO_2 structure of TaO_6 (**6_B**) nicely match the measured PIE, as shown in the dotted trace in Figure 7. This gives IE(TaO_6)=10.10±0.05 eV, consistent with the 10.16 eV upper limit from the linear fit. The calculated ionization energy of structure **6_B** is 10.01 eV, in agreement with experiment.

The photoionization experiments clearly suggest that structure **6_B** is the ground state of TaO_6. This is strongly supported by vibrational spectra of neutral TaO_6 in a cryogenic Ar matrix measured by Zhao et al.[15] They observe absorptions at 522.4, 889.4 and 944 cm^{-1}, which they assign to the Ta-O_2 stretch and the asymmetric and symmetric O-Ta-O stretches of the (η^2-O_2)(η^1-O_2) TaO_2 structure. Our calculated values (505, 893 and 967 cm^{-1}, respectively) are in excellent agreement. Note that the calculated vibrational frequencies of the bis(η^2-O_2) TaO_2

structure do not agree with the observed frequencies. In particular, no calculated frequency lies within 100 cm^{-1} of the observed strong band at 889.4 cm^{-1}.

Summary and Conclusions

The ionization energies of gas-phase TaO_x (x=3-6) have been determined, for the first time, from photoionization efficiency (PIE) spectra measured using single-photon VUV ionization at a synchrotron. The ionization energies are in the range of 10.0 to 10.65 eV, substantially higher than those of TaO or TaO_2. Calculated Franck-Condon factors based on separable, harmonic vibrations were sufficient to simulate PIEs for most of the oxides, but not for TaO_3. Calculations predict that the neutral and cation of TaO_3 have pseudo C_{3v} structures with low barriers to interconversion between three minima. Accurately reproducing the observed PIE's requires treating the antisymmetric Ta-O stretches as two coupled, anharmonic motions. For TaO_5 and TaO_6, the structure of the ground state was determined by comparing the measured PIEs to ones simulated for candidate, calculated structures. In each case, the calculations predict that the ground state is a superoxide structure that contains a Ta-O single bond. An alternate dioxygen structure, with a Ta=O double bond is predicted to be slightly higher in energy. In both cases, the measured PIE is clearly consistent with the dioxygen structure and not with the superoxide geometry.

As a solid, tantalum oxide has the formula Ta_2O_5, so tantalum is formally Ta^V. This oxidation state is retained in all of the gas-phase tantalum oxide clusters that contain sufficient oxygen atoms (i.e., TaO_x ($x\geq3$) and TaO_x^+ ($x\geq2$)). For the smaller clusters ($x\leq3$) this occurs by adjusting the number of Ta-O and Ta=O covalent bonds. The larger clusters also incorporate superoxide (O_2^-) and dioxygen (O_2) moieties. Ionization of the neutral oxides typically occurs with conversion of a Ta=O double bond to a single bond. This variety of oxygen-binding motifs means that binding energies of atomic and molecular oxygen in tantalum oxides vary greatly, and depend on the molecule's charge. As shown in Table 2, experiments and calculations agree that TaO, TaO_2 and their cations have extremely high O atom binding energies (>6 eV). Although binding energies for the higher oxides have not been measured, our calculations predict that they are substantially lower for TaO_3 (4.37 eV) and TaO_3^+ (2.67 eV). For the higher oxides, the most favorable dissociation channel is loss of O_2. Neutral TaO_4 is surprisingly stable, with a TaO_2-O_2 bond strength of 2.46 eV, while TaO_5 and TaO_6 bind O_2 much more weakly (0.77 and

0.64 eV, respectively). The binding energies of O_2 to TaO_2^+, TaO_3^+ and TaO_4^+ are all similar, and consistent with an electrostatic complex.

Acknowledgements MA and OK gratefully acknowledge support from the Director, Office of Energy Research, Office of Basic Energy Sciences, Chemical Sciences Division of the U.S. Department of Energy under contract No. DE-AC02-05CH11231. MP and RBM gratefully acknowledge the support of the National Science Foundation under awards CHE-0911225 and CHE-1300501.

References

1. Y. S. Chen, J. L. G. Fierro, T. Tanaka, I. E. Wachs, J. Phys. Chem. B 107 (2003) 5243.
2. I. E. Wachs, Y. Chen, J. M. Jehng, L. E. Briand, T. Tanaka, Catal. Today 78 (2003) 13.
3. D. A. Ruddy, T. D. Tilley, J. Am. Chem. Soc. 130 (2008) 11088.
4. P. J. Cordeiro, T. D. Tilley, Langmuir 27 (2011) 6295.
5. F. Dong, S. Heinbuch, S. G. He, Y. Xie, J. J. Rocca, E. R. Bernstein, J. Chem. Phys. 125 (2006) 164318.
6. S. Heinbuch, F. Dong, J. J. Rocca, E. R. Bernstein, J. Chem. Phys. 133 (2010) 174314.
7. M. Zhou, C. Wang, Z. Li, J. Zhuang, Y. Zhao, X. Zheng, K. Fan, Ang. Chem. Int. Ed. 49 (2010) 7757.
8. K. S. Molek, T. D. Jaeger, M. A. Duncan, J. Chem. Phys. 123 (2005) 144313.
9. K. A. Zemski, R. C. Bell, A. W. Castleman Jr., J. Phys. Chem. A 104 (2000) 5732.
10. C. J. Cheetham, R. F. Barrow, Trans. Faraday Soc. 63 (1967) 1835.
11. A. Al-Khalili, U. Hällsten, O. Launila, J. Mol. Spectrosc. 198 (1999) 230.
12. W. Weltner Jr., D. McLeod Jr., J. Chem. Phys. 42 (1965) 882.
13. M. Zhou, L. Andrews, J. Phys. Chem. A 102 (1998) 8251.
14. M. Chen, X. Wang, L. Zhang, M. Yu, Q. Qin, Chem. Phys. 242 (1999) 81.
15. Y. Zhao, X. Zheng, M. Zhou, Chem. Phys. 351 (2008) 13.
16. Y. Gong, M. Zhou, L. Andrews, Chem. Rev. 109 (2009) 6765.
17. J. M. Dyke, A. M. Ellis, M. Feher, A. Morris, A. J. Paul, J. C. H. Stevens, J. Chem. Soc. Faraday Trans. II 83 (1987) 1555.
18. W. Zheng, X. Li, S. Eustis, K. Bowen, Chem. Phys. Lett. 460 (2008) 68.
19. C. Nicolas, J. Shu, D. S. Peterka, L. Poisson, S. R. Leone, M. Ahmed, J. Am. Chem. Soc. 128 (2006) 220.
20. S. R. Leone, M. Ahmed, K. R. Wilson, Phys. Chem. Chem. Phys. 12 (2010) 6564.
21. A. Golan, M. Ahmed, J. Vis. Exp. 68 (2012) e50164.
22. K. M. Perera, R. B. Metz, O. Kostko, M. Ahmed, Ang. Chem. Int. Ed. 52 (2013) 888.
23. R. B. Metz, C. Nicolas, M. Ahmed, S. R. Leone, J. Chem. Phys. 123 (2005) 114313.
24. M. Citir, R. B. Metz, L. Belau, M. Ahmed, J. Phys. Chem. A 112 (2008) 9584.
25. M. J. Frisch, G. W. Trucks, H. B. Schlegel, G. E. Scuseria, M. A. Robb, J. R. Cheeseman, G. Scalmani, V. Barone, B. Mennucci, G. A. Petersson, H. Nakatsuji, M. Caricato, X. Li, H. P. Hratchian, A. F. Izmaylov, J. Bloino, G. Zheng, J. L. Sonnenberg, M. Hada, M. Ehara, K. Toyota, R. Fukuda, J. Hasegawa, M. Ishida, T. Nakajima, Y. Honda, O. Kitao, H. Nakai, T. Vreven, J. A. Montgomery Jr., J. E. Peralta, F. Ogliaro, M. Bearpark, J. J. Heyd, E. Brothers, K. N. Kudin, V. N. Staroverov, T. Keith, R. Kobayashi, J. Normand, K. Raghavachari, A. Rendell, J. C. Burant, S. S. Iyengar, J. Tomasi, M. Cossi, N. Rega, J. M. Millam, M. Klene, J. E. Knox, J. B. Cross, V. Bakken, C. Adamo, J. Jaramillo, R. Gomperts, R. E. Stratmann, O. Yazyev, A. J. Austin, R. Cammi, C. Pomelli, J. W. Ochterski, R. L. Martin, K. Morokuma, V. G. Zakrzewski, G. A. Voth, P. Salvador, J. J. Dannenberg, S. Dapprich, A. D. Daniels, O. Farkas, J. B. Foresman, J. V. Ortiz, J. Cioslowski, D. J. Fox, in ed., Gaussian, Inc., Wallingford, CT, Pittsburgh PA (2010.
26. D. Figgen, K. A. Peterson, M. Dolg, H. Stoll, J. Chem. Phys. 130 (2009) 164108.
27. S. Smoes, J. Drowart, C. E. Myers, J. Chem. Thermo. 8 (1976) 225.
28. M. G. Inghram, W. A. Chupka, J. Berkowitz, J. Chem. Phys. 27 (1957) 569.
29. E. K. Kazenas, A. A. Petrov, I. O. Samoilova, Russ. Metall. (Metally) 1994 (1994) 16.

30. Z. J. Wu, Y. Kawazoe, J. Meng, J. Mol. Struct.-Theochem 764 (2006) 123.
31. C. S. Hinton, F. X. Li, P. B. Armentrout, Int. J. Mass Spectrom. 280 (2009) 226.
32. C. S. Hinton, M. Citir, M. Manard, P. B. Armentrout, Int. J. Mass Spectrom. 308 (2011) 265.
33. B. Simard, P. Kowalczyk, A. M. James, Phys. Rev. A 50 (1994) 846.
34. R. Wesendrup, H. Schwarz, Ang. Chem. Int. Ed. 34 (1995) 2033.
35. H.-J. Zhai, W.-J. Chen, S.-J. Lin, X. Huang, L.-S. Wang, J. Phys. Chem. A 117 (2013) 1042.
36. C. A. Taatjes, D. L. Osborn, T. A. Cool, K. Nakajima, Chem. Phys. Lett. 394 (2004) 19.
37. A. Weaver, D. W. Arnold, S. E. Bradforth, D. M. Neumark, J. Chem. Phys. 94 (1991) 1740.
38. J. F. Stanton, J. Chem. Phys. 126 (2007) 134309.

Tables

Table 1. Ionization energies of TaO_x (x=0-6), in eV. Theoretical values are at the B3LYP/aug-cc-pVTZ level.

Species	Experiment	Theory
Ta	7.55	7.48
TaO	8.61±0.02[a]	7.93
TaO_2	8.5±0.5[b]; 9.0±0.5[c]	8.80
TaO_3	10.65±0.05	10.50
TaO_4 (adiabatic)	10.36±0.1[d]	10.31
TaO_4 (to (η^2-O_2) TaO_2^+, **4c_B**)	10.53±0.05	10.48
TaO_5 ((η^2-O_2) TaO_3, **5_A)**	---	10.41
TaO_5 ((η^1-O_2) TaO_3, **5_B)**	10.0±0.2	10.11
TaO_6 (bis (η^2-O_2) TaO_2, **6_A**)	---	10.18
TaO_6 ((η^2-O_2)(η^1-O_2) TaO_2^+, **6_B**)	10.10±0.05	10.01

a. Ref. [17]
b. Ref. [27]
c. Ref. [28]
d. Estimated, see text for details.

Table 2. Tantalum oxide bond strengths, in eV. All values are at 0 K. Theoretical values are at the B3LYP/aug-cc-pVTZ level.

	Experiment		Theory	
Bond	Neutral	Cation	Neutral	Cation
Ta-O	8.19[a], 8.30±0.13[b]	7.01±0.12[c]	8.12	7.66
(TaO)-O	6.63[a], 6.87±0.23[b]	6.08±0.12[c]	7.04	6.18
(TaO_2)-O			4.37	2.67
(TaO_2)-O_2			2.46	0.96
(TaO_3)-O_2			0.77	0.85
(TaO_4)-O_2			0.64	0.76

a. Ref. [29]
b. Ref. [27]
c. Ref. [32]

Table 3. Reference C_{3v} geometry of TaO_3 and TaO_3^+ in Cartesian coordinates, along with the form of the antisymmetric stretch vibrations, in Cartesian displacements. All distances in Å. The reduced mass of the vibrations is 18.43 amu.

	Reference geometry			Q_{3a}			Q_{3b}		
	x	y	z	x	y	z	x	y	z
Ta	0.0000	0.0000	0.1752	0.0000	0.1215	0.0000	0.1215	0.0000	0.0000
O	0.0000	1.6385	-0.5330	0.0000	-0.6586	0.3959	-0.2583	0.0000	0.0000
O	-1.4190	-0.8192	-0.5330	-0.1727	-0.3581	-0.1984	-0.5582	-0.1732	-0.3431
O	1.4190	-0.8192	-0.5330	0.1727	-0.3581	-0.1984	-0.5582	0.1732	0.3431

Table 4. Fitting parameters for antisymmetric stretching potentials of TaO_3 and TaO_3^+ (equation 2).

	TaO_3	TaO_3^+
q ($cm^{-1}/Å^3$)	5.114×10^5	2.210×10^5
k ($cm^{-1}/Å^2$)	-4.725×10^4	1.299×10^5
a ($cm^{-1}/Å$)	2.989×10^3	1.559×10^4
b ($cm^{-1}/Å^4$)	-7.791×10^5	4.310×10^5
c ($cm^{-1}/Å^3$)	3.563×10^5	-1.766×10^4
d ($cm^{-1}/Å^2$)	3.716×10^3	-2.037×10^4

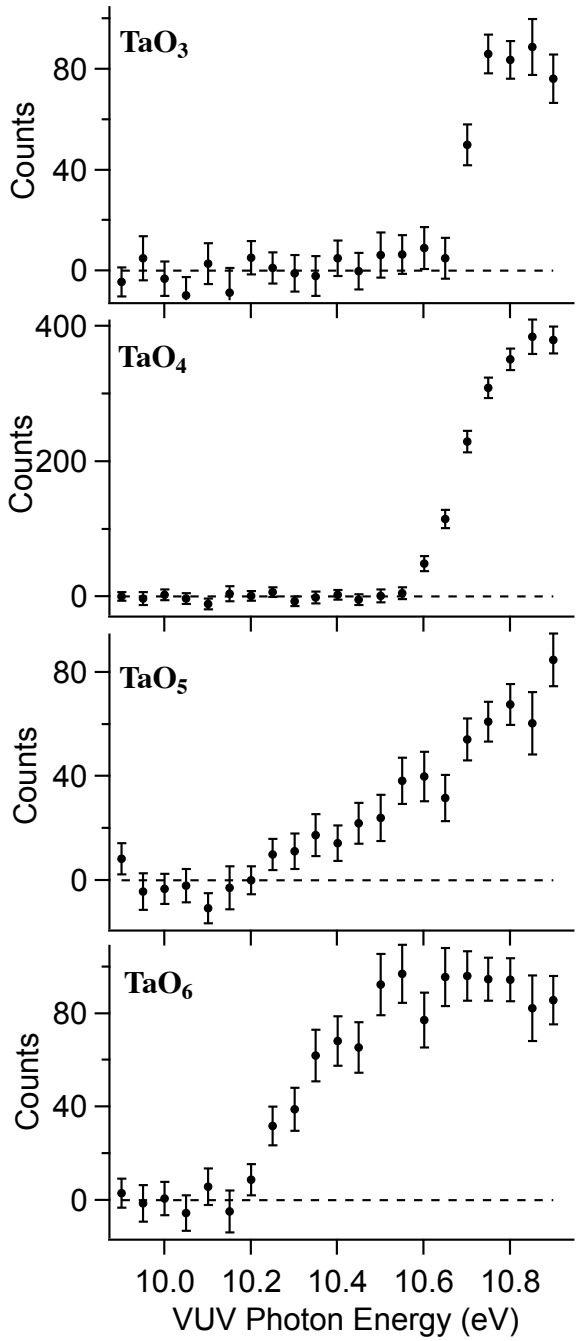

Figure 1

Figure 1. Photoionization efficiency spectra of TaO_x (x=3-6).

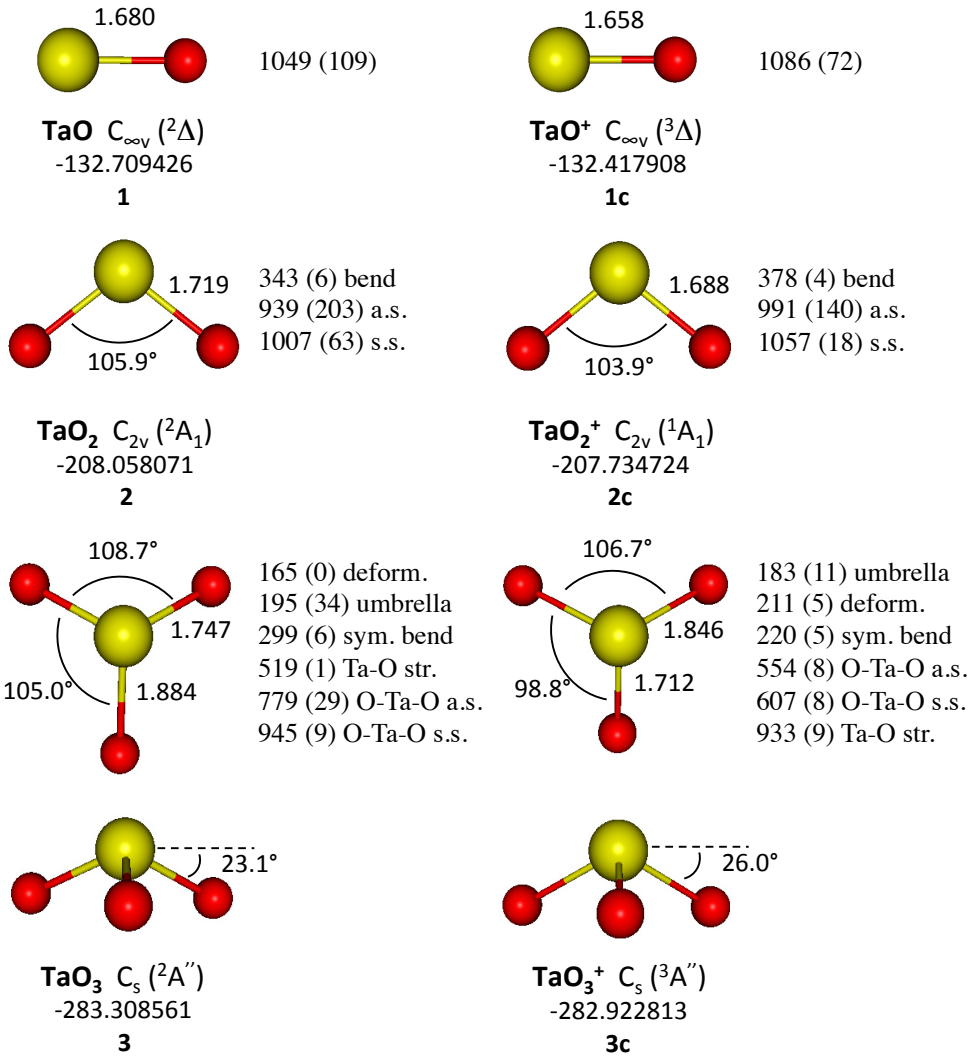

Figure 2

Figure 2. Structures, energies and harmonic vibrational frequencies of TaO_x and TaO_x^+ (x=1-3) calculated at the B3LYP/aug-cc-pVTZ level. Energies are in hartree and include zero-point energy; vibrational frequencies are in cm^{-1} and are unscaled. IR absorption intensities, in km/mol are in parentheses. Additional results: O (^3P): -75.0898795; O_2 ($^3\Sigma$): -150.380913 (r_e=1.206 Å, ω_e=1626 cm^{-1}); O_2^-: r_e=1.343 Å, ω_e=1164 cm^{-1}); Ta (^4F): -57.3025188; Ta^+ (^5F): -57.046467.

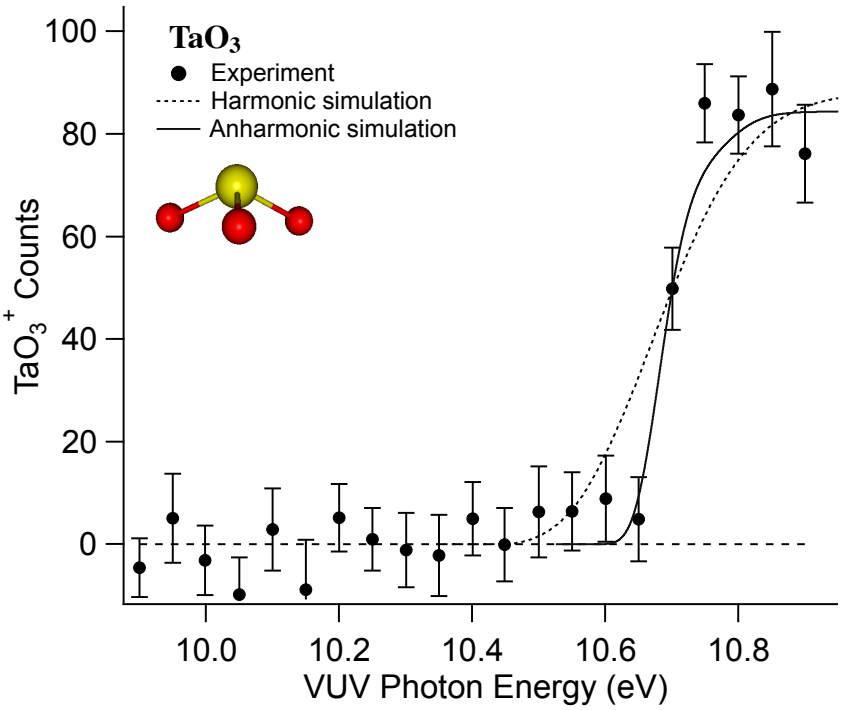

Figure 3

Figure 3. Photoionization efficiency spectrum of TaO_3, along with simulated spectra assuming separable, harmonic antisymmetric stretch potentials (dotted line) and the two-dimensional coupled, anharmonic antisymmetric stretch potentials shown in Fig. 4 (solid line), which gives IE(TaO_3)=10.65±0.05 eV.

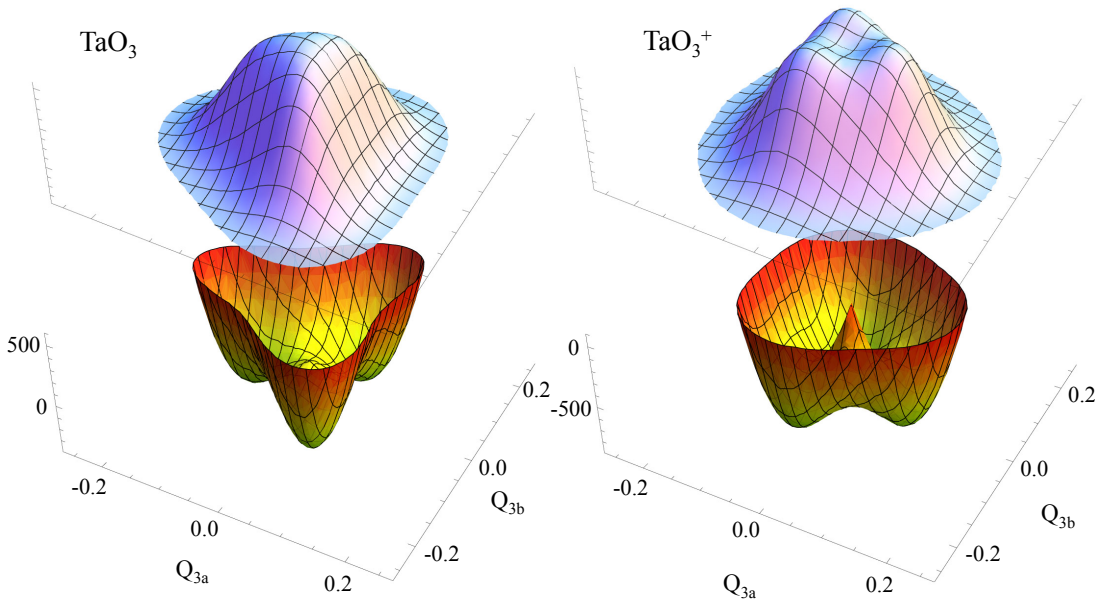

Figure 4

Figure 4. Two-dimensional potential energy surfaces and ground state wavefunctions for the antisymmetric stretch vibrations of TaO_3 and TaO_3^+. The vertical axis for the potentials is in cm^{-1}.

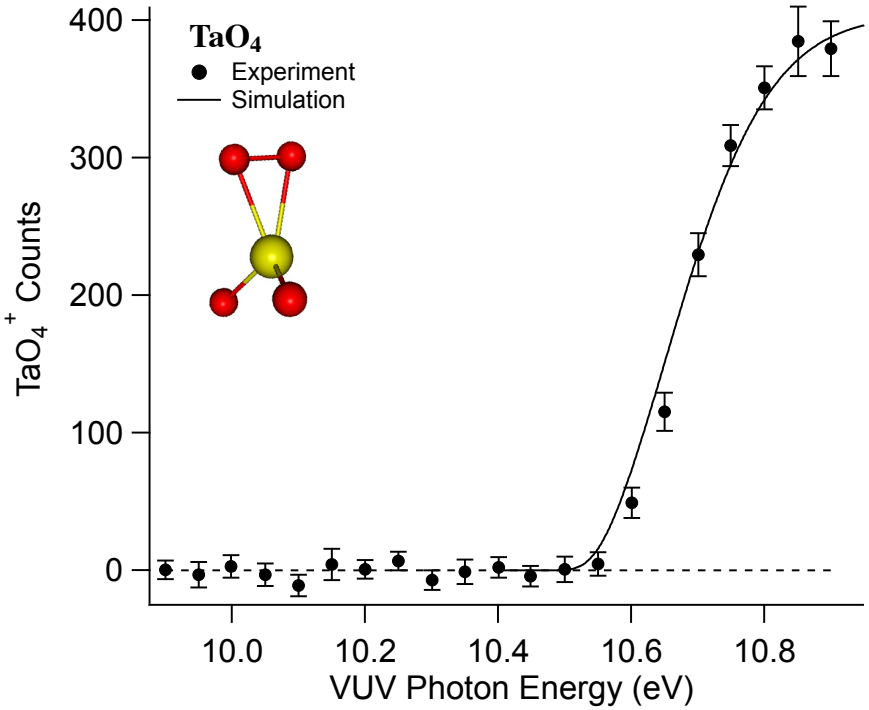

Figure 5

Figure 5. Photoionization efficiency spectrum of TaO_4, along with the simulated spectrum for ionization to the $^3A'$ (superoxide) state of TaO_4^+ at an ionization energy of 10.53±0.05 eV.

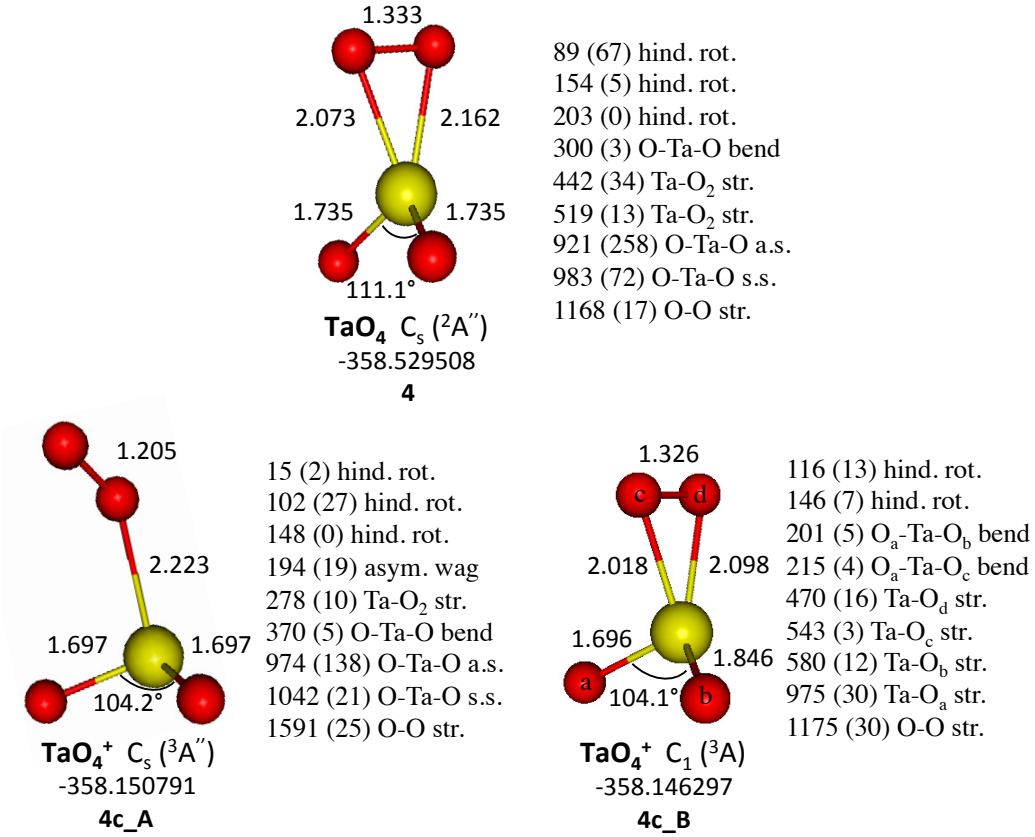

Figure 6

Figure 6. Structures, energies and harmonic vibrational frequencies of TaO_4 and two isomers of TaO_4^+ calculated at the B3LYP/aug-cc-pVTZ level. Energies are in hartree and include zero-point energy; vibrational frequencies are in cm^{-1} and are unscaled. IR absorption intensities, in km/mol are in parentheses.

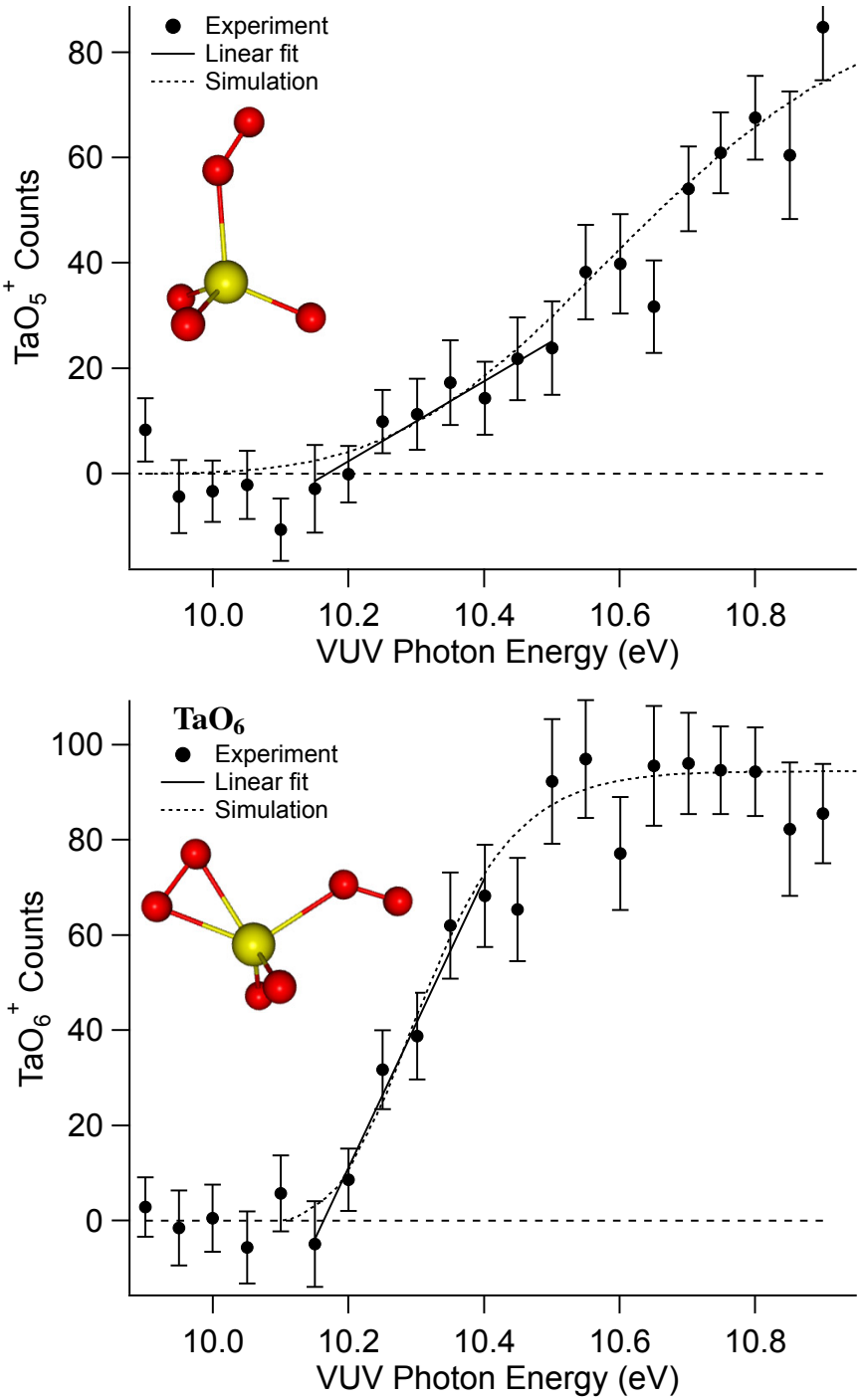

Figure 7

Figure 7. Photoionization efficiency spectra of TaO_5 and TaO_6 along with linear fits to the onset and simulated spectra for ionization from structures **5_B** and **6_B**.

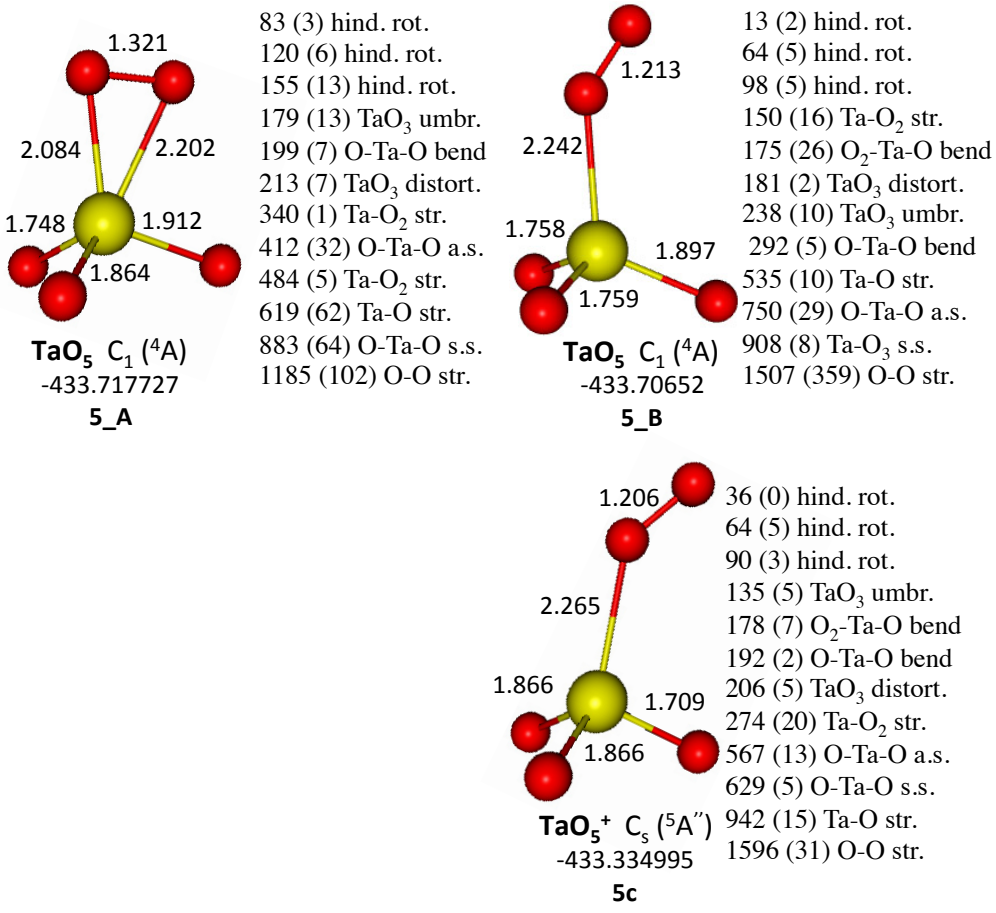

Figure 8

Figure 8. Structures, energies and harmonic vibrational frequencies of TaO_5 and TaO_5^+ calculated at the B3LYP/aug-cc-pVTZ level. Energies are in hartree and include zero-point energy; vibrational frequencies are in cm^{-1} and are unscaled.

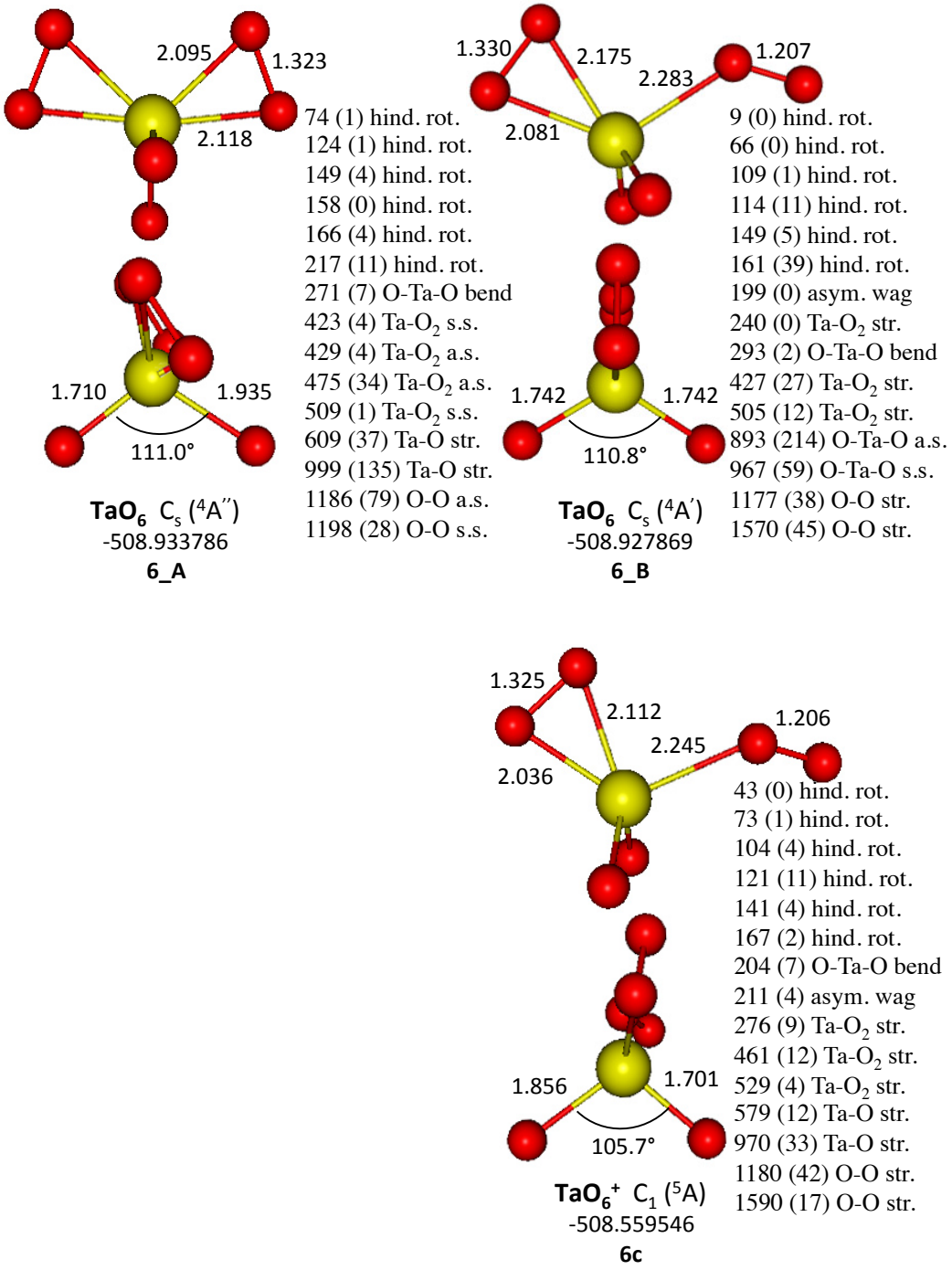

Figure 9

Figure 9. Structures, energies and harmonic vibrational frequencies of TaO_6 and TaO_6^+ calculated at the B3LYP/aug-cc-pVTZ level. Energies, in hartree, include zero-point energy; vibrational frequencies, in cm^{-1}, are unscaled.